Journal of Power Sources 242 (2013) 65–69

Contents lists available at SciVerse ScienceDirect

Journal of Power Sources

journal homepage: www.elsevier.com/locate/jpowsour

Short communication

Reduced graphene oxide film as a shuttle-inhibiting interlayer in a lithium–sulfur battery

Xuefeng Wang, Zhaoxiang Wang*, Liquan Chen

Key Laboratory for Renewable Energy, Beijing Key Laboratory for New Energy Materials and Devices, National Laboratory for Condensed Matter Physics, Institute of Physics, Chinese Academy of Sciences, China

HIGHLIGHTS

- A reduced graphene oxide (rGO) based interlayer is used as a shuttle inhibitor.
- The rGO interlayer improves the cycling performance of the Li–S cell significantly.
- Functional groups on the rGO help to anchor the sulfur and polysulfides.
- Compromise is required between anchoring sulfides and building electrolyte channels.

GRAPHICAL ABSTRACT

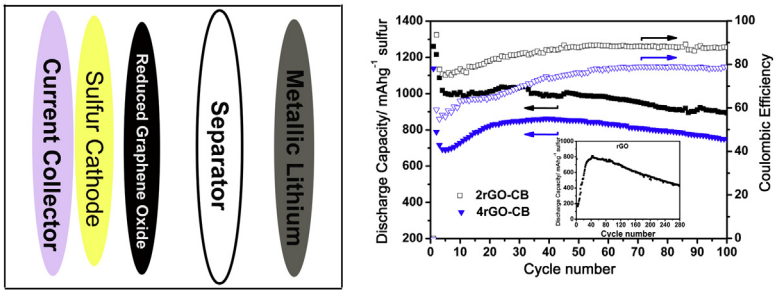

ARTICLE INFO

Article history:
Received 2 April 2013
Received in revised form
14 May 2013
Accepted 15 May 2013
Available online 25 May 2013

Keywords:
Energy storage
Functional groups
Strong absorption
Channels

ABSTRACT

A reduced graphene oxide (rGO) based film is sandwiched between a sulfur cathode and the separator, acting as a shuttle inhibitor to the sulfur and polysulfides. The lithium–sulfur cell with such a configuration shows an initial discharge capacity of 1260 mAh g^{-1} and the capacity remains at 895 mAh g^{-1} after 100 cycles. The excellent electrochemical performance of the cell is attributed to both the functional groups on the rGO sheets that anchor the sulfur and polysulfides and the carbon additive that helps to produce channels for the electrolyte and polysulfide to enter.

1. Introduction

Sulfur is abundant, cheap and nontoxic. The rechargeable lithium batteries with sulfur cathode (lithium–sulfur or Li–S battery) are expected to deliver a theoretical energy density up to 2600 Wh kg^{-1} [1], suitable for electric vehicles that can drive 500 km or more between two charges. However, the insulating nature of the sulfur and the high solubility of the lithium polysulfides in the liquid electrolyte impede the commercialization of the Li–S batteries. A variety of strategies have been proposed to improve the electrochemical performance of the Li–S batteries by special designs of the cathode structure, electrolyte composition and anode protection.

Most of the attention on the sulfur cathode has been focused on confining the sulfur in/on various forms of carbon, such as graphene [2–4], carbon nanotubes [5,6], carbon spheres [7–9], mesoporous carbons [10–12], etc. Archer et al. [13] encapsulated the sulfur into hollow carbon spheres. The cell with 70 wt% sulfur in the composite manifests an initial specific discharge capacity of 1071 mAh g^{-1} and maintains a reversible capacity of 974 mAh g^{-1} (at a rate of 0.5 C) with 94% coulombic efficiency after 100 cycles.

* Corresponding author.
E-mail address: zxwang@iphy.ac.cn (Z. Wang).

0378-7753/$ – see front matter © 2013 Elsevier B.V. All rights reserved.
http://dx.doi.org/10.1016/j.jpowsour.2013.05.063

However, the preparation of hollow carbon spheres is complicated. In terms of the electrolyte, solid-state electrolyte such as polymer based electrolyte [14–16], inorganic-ceramic electrolytes (Li_2S–P_2S_5) [17,18] and ionic liquid [19–21] are explored to replace the liquid electrolyte. In addition, additives such as $LiNO_3$ [22,23], LiBOB [24], P_2S_5 [25] that help to form protective films on the lithium metal were tried to increase the coulombic efficiency and elongate the cycle life of the battery. However, the obtained success is quite limited. More effective approaches have to be set up to improve the electrochemical performance of the lithium–sulfur battery.

Recently, Manthiram and co-workers inserted an interlayer between the sulfur cathode and separator, such as a free-standing MWCNT [26] and microporous carbon paper [27]. The carbon interlayer facilitates the absorption of soluble polysulfide and makes them available for re-utilization during cycling. This strategy significantly improves both the utilization of the active material and the capacity retention of the cell. Even earlier, Kim et al. [28] increased the sulfur utilization by sputtering a thin layer (18 nm thick) of amorphous carbon on the sulfur cathode. However, the capacity fading was still quick due to damage of the carbon coating layer during cycling.

Clearly, a referable interlayer with stronger absorption to the sulfur and polysulfide is preferred. In this respect, reduced graphene oxide (rGO) is an ideal candidate of absorbent. The oxygen functional groups on its basal planes and edges and the structural defects provide it with strong anchoring points [29,30] while its two-dimensional (2D) sheet-like structure promotes the formation of self-assembled films. Herein, rGO based films are sandwiched between a sulfur cathode and the separator as a shuttle inhibitor. Electrochemical evaluation indicates that the rGO based interlayer enhances the cycling performance of the Li–S battery.

2. Experimental

Graphite oxide (GO) was prepared from natural graphite powder by a modified Hummers method [29]. In a typical experiment, 1 g graphite powder and 0.5 g sodium nitrate ($NaNO_3$) were added into 70 ml concentrated H_2SO_4 in an ice bath, followed by the addition of 3 g $KMnO_4$. The mixture was stirred for 2 h and then diluted with de-ionized water. After 24 h stirring, 30% H_2O_2 was added into the solution until the color of the mixture became brilliant yellow. Repeated centrifugation and washing were performed to clean out the residual salt. The as-prepared GO was ultrasonically dispersed in de-ionized water for 1 h. Ketjen Black (a conductive carbon black, CB) was then added into the slurry and mixed ultrasonically for another 1 h to form a GO–CB suspension. Films of the GO and the GO–CB composite were fabricated by suction-filtering the above suspensions. After heat-treatment at 155 °C in a vacuum oven, the GO was reduced and dried. Therefore, in the following description and discussion, reduced graphene oxide (rGO) and rGO–CB were denoted in this paper.

The structure of the rGO based films were characterized by powder X-ray diffraction (Philips, Holland) with Cu Kα1 radiation ($\lambda = 1.5405$ Å). The morphology of the interlayer film was observed on an FEI XL30 Sirion FEG digital scanning electron microscope. Fourier-transformed infrared (FTIR) spectra of the powder dispersed in dry KBr were recorded on a Bruker VERTEX 70v spectrometer.

The working electrode (the sulfur cathode sheet) was prepared by pressing a mixture of sulfur (80 wt %), carbon nanotubes (15 wt %) (XF NANO, Nanjing, China) and polytetrafluorethylene (PTFE) (5 wt %) into an Al mesh (current collector). CR2032 coin cells were assembled in an Ar-filled glove box with Li foil as the counter electrode, 1 mol L^{-1} of LiTFSI in 1,3-dioxolane (DOL) and 1,2-dimethoxyethane (DME) (1:1 in volume) (BASF Battery Materials, Suzhou, China) as the electrolyte. Between the Celgard 2300 separator and the S-based working electrode lies the rGO or rGO–CB interlayer. Typically, the mass of the sulfur in the sulfur cathode and that of the interlayer film (rGO or rGO–CB) are both around 3 mg. The cells were charged and discharged at a current density of 167.5 mA g^{-1} (unless otherwise specified) between 1.0 and 3.0 V on a Land BT2000 battery tester (Wuhan, China) at room temperature. The cyclic voltammetry (CV) was conducted on a CHI600D electrochemical workstation (Shanghai, China) at a scan rate of 0.1 mV s^{-1}.

3. Results and discussion

The as-prepared GO film shows wide diffraction peaks at about 22.5° (2θ) (Fig. 1a). After heat treatment at 155 °C in vacuum, it is reduced to rGO; the diffraction peaks become sharper. It is reported that the conductivity of GO increases by two orders of magnitude when it is transformed to rGO [31]. SEM imaging indicates that the surface of the self-assembled rGO film is rather smooth (Fig. 1b).

The test cell with a rGO interlayer shows an initial discharge capacity of 773 mAh g^{-1}. The discharge capacity increases gradually in the subsequent 40 cycles and reaches a maximum of about 800 mAh g^{-1}. The potential profile of the cell indicates that the gradual increase of the capacity corresponds to an activation process. We suggest that the activation process as follows. The polysulfides produced in the previous cycles dissolute into the electrolyte, attach or are adsorbed on the of rGO surface for further reaction. Then with the continuous cycling, more and more polysulfides and electrolyte molecules permeate into the tightly stacked rGO sheets and the sulfur utilization of the increases. After 280 cycles, the cell shows a discharge capacity of 427 mAh g^{-1} and coulombic efficiency of ca. 60%.

In order to shorten the activation time and improve the cycling stability of sulfur cathode, CB was introduced into the rGO interlayer. For comparison, composite films with mass ratios of rGO:CB = 4:1 and 2:1 are prepared and denoted as 4rGO–CB and 2rGO–CB, respectively. SEM imaging shows that the surface of the rGO–CB film is much rougher than the CB-free film. Meanwhile, the structure of the rGO–CB film becomes looser and porous, providing channels for the permeation of the electrolyte and polysulfides. Further increasing the CB content in the composite makes it difficult to form a self-assembled film.

Fig. 2 depicts the electrochemical performance of the cell with different rGO–CB composite interlayer. The risen voltage plateau of the initial discharge profile indicates the reduced polarization of the cell with rGO–CB interlayer in comparison with that using a pure rGO interlayer. The cyclic voltammetry (CV) exhibits the reaction of sulfur in the first two cycles (Fig. 2b). The broad reduction peaks at about 2.2 V, 1.97 and 1.8 V in the initial cycle move to 2.25 V, 2.01 V and 1.77 V, respectively, in the 2nd cycle. Only one broad oxidation peak is observed at about 2.55 V; it does not change in the 2nd cycle. These redox features are consistent with the potential profiles.

The cycling performance of the cells with a rGO–CB interlayer is presented in Fig. 2c. Addition of CB in the rGO interlayer indeed remarkably shortens the activation time of the cell and improves both the capacity stability and coulombic efficiency of the cell. The discharge capacity of the cell with 4rGO–CB interlayer is 1139 mAh g^{-1} in the initial cycle and remains at 749 mAh g^{-1} after 100 cycles. In comparison, the cell with the 2rGO–CB interlayer shows an initial discharge capacity of 1260 mAh g^{-1} and maintains at 894 mAh g^{-1} after 100 cycles. The coulombic efficiency reaches ca. 90% in a few cycles. The improvement of the rate performance (Fig. 2d) is significant as well. When the current density increases to 1600 mA g^{-1}, the cell with the 2rGO–CB interlayer delivers a

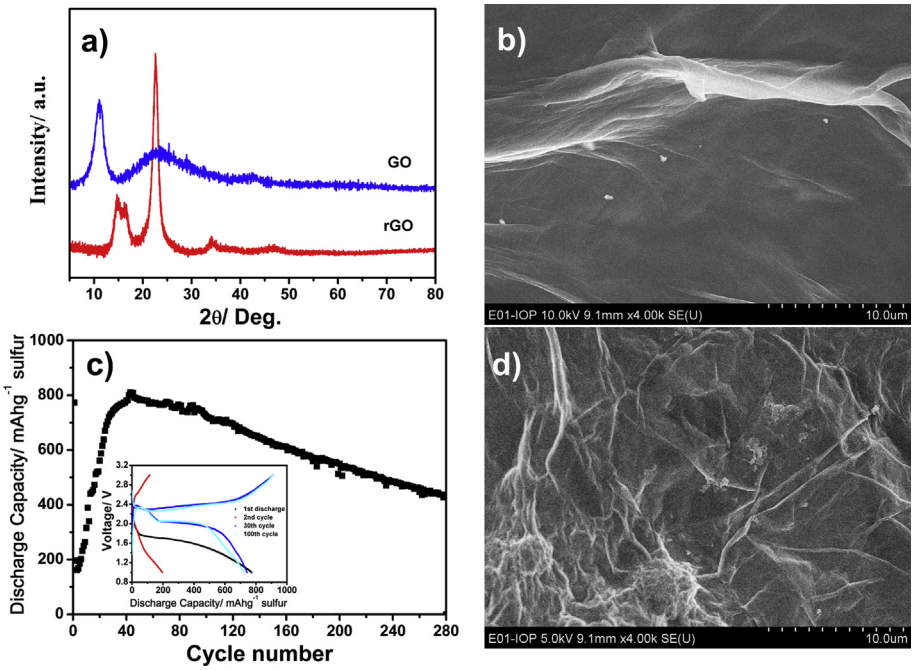

Fig. 1. The XRD patterns of the as-prepared GO and rGO films (a), the SEM imaging of a fresh rGO film (b), the cycling performance of a Li–S cell with a rGO interlayer (c), and the SEM imaging of an as-prepared 2rGO–CB composite film (d). The inset in (c) is for the potential profile of some selected cycles of a cell with rGO interlayer.

reversible capacity of 656 mAh g^{-1}. Even when a 3200 mA g^{-1} current density is applied, a capacity of 518 mAh g^{-1} is obtained. In general, the performance of the cell with the 2rGO–CB interlayer is better than that the cell with the 4rGO–CB interlayer.

SEM imaging shows that the surface of the 2rGO–CB interlayer surface (Fig. 3a and b) becomes smooth after cycling. Elemental mapping (Fig. 3c) indicates that the distribution of sulfur is homogeneous. Fourier transformed infrared (FTIR) spectroscopy (Fig. 3d) shows that, in comparison with the fresh 2rGO–CB film, the carboxyl C–O bonds (1586, 1404 cm^{-1}), carbonyl C=O (1732 cm^{-1}) bonds disappear while the S–S bonds (447 cm^{-1}), carbonate CO_3^{2-} bonds (1512, 868 cm^{-1}) emerge after the cell is cycled. Apparently the S–S bonds come from the sulfur or polysulfides anchored on the interlayer. Considering the simultaneous disappearance (the carboxyl C–O bonds at 1404 cm^{-1} and carbonyl C=O bonds at 1732 cm^{-1}) and appearance (the carbonate) of the bonds, we believe that during cycling, the carboxyl and carbonyl group can be further oxidized to carbonate groups with the

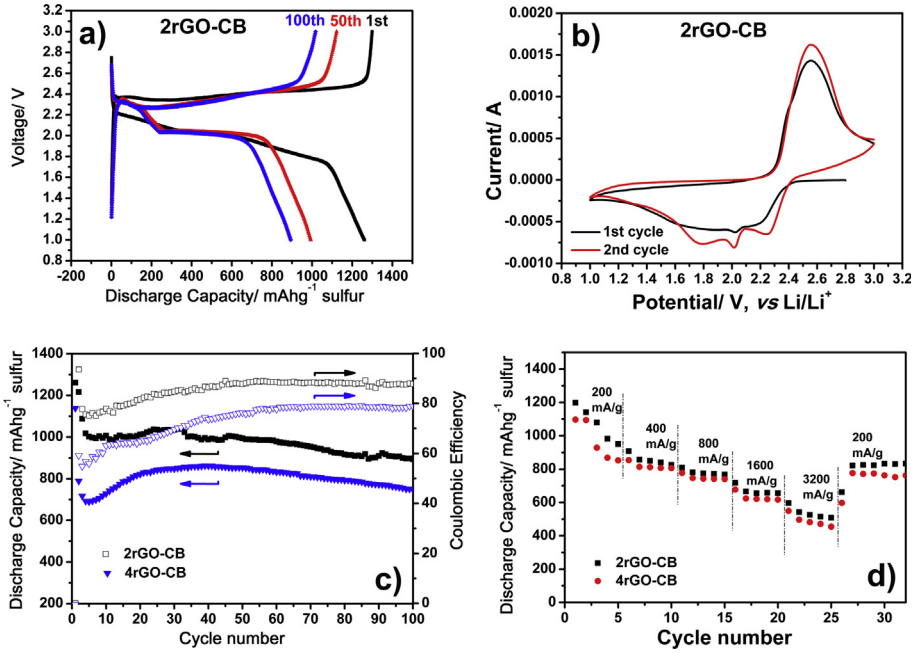

Fig. 2. The electrochemical performances of the cells with rGO–CB composite interlayer: (a) the potential profile of some selected cycles of the 2rGO–CB cell, (b) the cyclic voltammograms in the first two cycles, (c) the cycling performance, and (d) the rate performance of the cells with different rGO–CB composite interlayers.

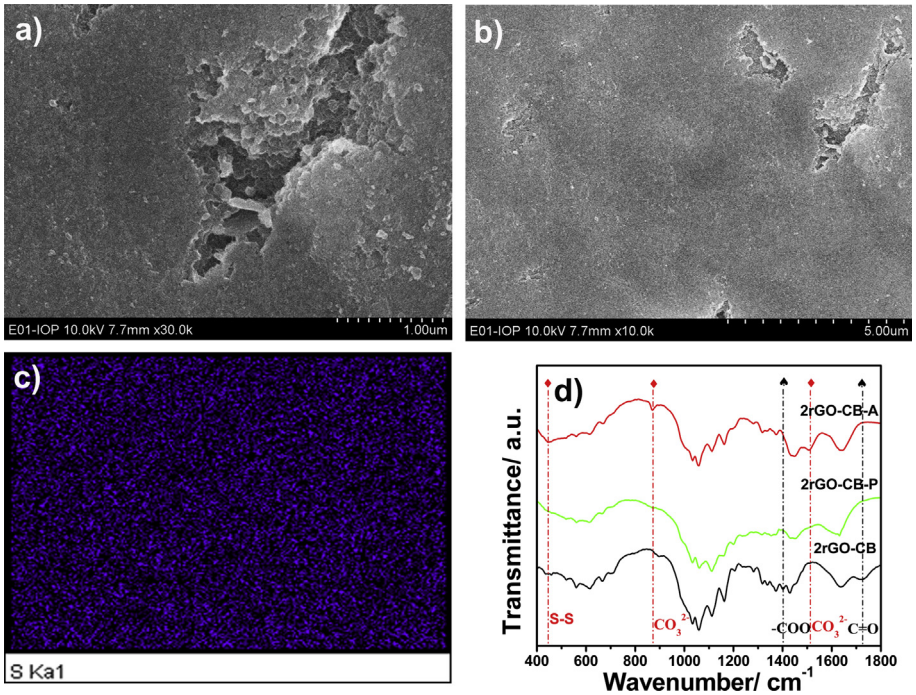

Fig. 3. The SEM images of 2rGO–CB after 113 cycles at a current density of 165 mA g^{-1} (a and b), the elemental sulfur distribution (c), and the FTIR spectrum of 2rGO–CB film before (2rGO–CB), after cycling (2rGO–CB–A) and 2rGO–CB cathode after cycling under the same condition (2rGO–CB–P) (d).

assistance of the polysulfides. This suggestion is supported with the fact that carbonate is not detected in the 2rGO–CB cathode after cycling under the same condition. Furthermore, the epoxy and hydroxyl groups on the 2rGO–CB films can enhance the binding of S to the C–C bonds due to the induced ripples by the functional groups, according to Zhang et al. [31]. Therefore, the rGO can strongly anchor the sulfur and polysulfides.

The above results show that with a rGO interlayer, the cycling stability and coulombic efficiency of the cell can be improved due to the strong interactions between the functional groups of the rGO and the sulfur and polysulfides. However, the sheet-like structure of the graphene makes it difficult for the electrolyte and polysulfides to enter between the rGO sheets, resulting in longer activation time, lower utilization of the active sulfur. That is, the rGO sheets characteristic of high specific surface area, abundant surface functional groups cannot take their functions because these sheets are too tightly stacked together, leaving few gaps for the electrolyte and the polysulfides to enter. Insertion of CB particles enlarges the gaps between the rGO sheets and creates more channels or pores for the electrolyte and polysulfides to permeate. This is different from the case of the carbon nanotube based interlayer as Manthiram et al. reported [26]. A mass ratio of rGO:CB = 4:1 is sufficient to produce more channels and effectively shorten the activation time. Higher content of CB in the interlayer can further improve the utilization of the active materials. However, too much CB in the rGO–CB composite makes it difficult to prepare an integrated interlayer film. Mass ratio of rGO:CB = 2:1 seems to be the maximum content of CB that makes a compromise between the electrochemical performance and the sample preparation in this work.

4. Conclusions

Reduced graphene oxide based films are sandwiched between a sulfur cathode and the separator to anchor the sulfur and the polysulfides so as to inhibit/suppress the shuttle effect. The functional groups such as epoxy and carboxyl on the rGO are beneficial to retaining and accommodating the sulfur and polysulfides. The rGO based film can promote the utilization of the active materials. The cell with a 2rGO–CB interlayer has an initial discharge capacity of 1260 mAh g^{-1} and remains 895 mAh g^{-1} after 100 cycles. Considering the significantly improved performance of the Li–S cell with a rGO–CB composite interlayer, the commercial availability of the CB, and the ease of fabricating rGO and rGO–CB film, the configuration of our rGO–CB interlayer inserted Li–S cell throws a light on the design of advanced Li–S cells.

Acknowledgments

This work was financially supported by the National 973 Program of China (2009CB220100).

References

[1] P.G. Bruce, S.A. Freunberger, L.J. Hardwick, J.M. Tarascon, Nat. Mater. 11 (2012) 19–29.
[2] H. Wang, Y. Yang, Y. Liang, J.T. Robinson, Y. Li, A. Jackson, Y. Cui, H. Dai, Nano Lett. 11 (2011) 2644–2647.
[3] S. Evers, L.F. Nazar, Chem. Commun. 48 (2012) 1233–1235.
[4] L.C. Yin, J.L. Wang, F.J. Lin, J. Yang, Y. Nuli, Energy Environ. Sci. 5 (2012) 6966–6972.
[5] J.j. Chen, Q. Zhang, Y.n. Shi, L.l. Qin, Y. Cao, M.s. Zheng, Q.f. Dong, Phys. Chem. Chem. Phys. 14 (2012) 5376–5382.
[6] F. Wu, J.Z. Chen, L. Li, T. Zhao, R.J. Chen, J. Phys. Chem. C 115 (2011) 24411–24417.
[7] C. Zhang, H.B. Wu, C. Yuan, Z. Guo, X.W. Lou, Angew. Chem. Int. Ed. Engl. 51 (2012) 9592–9595.
[8] X. Liang, Z. Wen, Y. Liu, H. Zhang, L. Huang, J. Jin, J. Power Sources 196 (2011) 3655–3658.
[9] B. Zhang, X. Qin, G.R. Li, X.P. Gao, Energy Environ. Sci. 3 (2010) 1531–1537.
[10] G.C. Li, G.R. Li, S.H. Ye, X.P. Gao, Adv. Energy Mater. 2 (2012) 1238–1245.
[11] S. Wei, H. Zhang, Y. Huang, W. Wang, Y. Xia, Z. Yu, Energy Environ. Sci. 4 (2011) 736–740.
[12] X. Ji, K.T. Lee, L.F. Nazar, Nat. Mater. 8 (2009) 500–506.
[13] N. Jayaprakash, J. Shen, S.S. Moganty, A. Corona, L.A. Archer, Angew. Chem. Int. Ed. 50 (2011) 5904–5908.
[14] J.L. Wang, J. Yang, J.Y. Xie, N.X. Xu, Y. Li, Electrochem. Commun. 4 (2002) 499–502.

[15] X. Yu, J. Xie, J. Yang, K. Wang, J. Power Sources 132 (2004) 181–186.
[16] C.W. Park, H.S. Ryu, K.W. Kim, J.H. Ahn, J.Y. Lee, H.J. Ahn, J. Power Sources 165 (2007) 450–454.
[17] T. Kobayashi, Y. Imade, D. Shishihara, K. Homma, M. Nagao, R. Watanabe, T. Yokoi, A. Yamada, R. Kanno, T. Tatsumi, J. Power Sources 182 (2008) 621–625.
[18] M. Nagao, A. Hayashi, M. Tatsumisago, Electrochim. Acta 56 (2011) 6055–6059.
[19] L.X. Yuan, J.K. Feng, X.P. Ai, Y.L. Cao, S.L. Chen, H.X. Yang, Electrochem. Commun. 8 (2006) 610–614.
[20] J. Wang, S. Chew, Z. Zhao, S. Ashraf, D. Wexler, J. Chen, S. Ng, S. Chou, H. Liu, Carbon 46 (2008) 229–235.
[21] A.S. Fisher, M.B. Khalid, M. Widstrom, P. Kofinas, J. Power Sources 196 (2011) 9767–9773.
[22] X. Liang, Z.Y. Wen, Y. Liu, M.F. Wu, J. Jin, H. Zhang, X.W. Wu, J. Power Sources 196 (2011) 9839–9843.
[23] S.S. Zhang, Electrochim. Acta 70 (2012) 344–348.
[24] S. Xiong, X. Kai, X. Hong, Y. Diao, Ionics 18 (2011) 249–254.
[25] Z. Lin, Z. Liu, W. Fu, N.J. Dudney, C. Liang, Adv. Funct. Mater. 23 (2013) 1064–1069.
[26] Y.S. Su, A. Manthiram, Chem. Commun. 48 (2012) 8817–8819.
[27] Y.S. Su, A. Manthiram, Nat. Commun. 3 (2012) 1166.
[28] Y.-J. Choi, Y.-D. Chung, C.-Y. Baek, K.-W. Kim, H.-J. Ahn, J.-H. Ahn, J. Power Sources 184 (2008) 548–552.
[29] J. Kim, L.J. Cote, J. Huang, Acc. Chem. Res. 45 (2012) 1356–1364.
[30] I.V. Lightcap, P.V. Kamat, Acc. Chem. Res. (2012).
[31] L. Ji, M. Rao, H. Zheng, L. Zhang, Y. Li, W. Duan, J. Guo, E.J. Cairns, Y. Zhang, J. Am. Chem. Soc. 133 (2011) 18522–18525.